

# Polarized QPOs from the INTEGRAL polar IGRJ14536-5522 (=Swift J1453.4-5524).

Stephen B. Potter<sup>1</sup>, David A. H. Buckley<sup>1</sup>, Darragh O’Donoghue<sup>1</sup>, Encarni Romero–Colmenero<sup>1</sup>, James O’Connor<sup>1</sup>, Piet Fourie<sup>1</sup>, Geoff Evans<sup>1</sup>, Craig Sass<sup>1</sup>, Lisa Crause<sup>1</sup>, Martin Still<sup>4,5</sup>, O. W. Butters<sup>2,6</sup>, A.J. Norton<sup>2</sup> and Koji Mukai<sup>3</sup>

<sup>1</sup>South African Astronomical Observatory, PO Box 9, Observatory 7935, Cape Town, South Africa

<sup>2</sup>Department of Physics and Astronomy, The Open University, Walton Hall, Milton Keynes, MK7 6AA, UK.

<sup>3</sup>CRESSST and X-ray Astrophysics Laboratory NASA/GSFC, Greenbelt, MD 20771, USA; Department of Physics, University of Maryland, Baltimore county, 1000 Hilltop Circle, Baltimore, MD 21250, USA;

<sup>4</sup>Mullard Space Science Laboratory, University College London, Holmbury St Mary, Dorking, Surrey RH5 6NT

<sup>5</sup>NASA Ames Research Center, Moffett Field, CA 94035, USA

<sup>6</sup>Department of Physics and Astronomy, University of Leicester, Leicester, LE1 7RH, UK

## ABSTRACT

We report optical spectroscopy and high speed photometry and polarimetry of the INTEGRAL source IGRJ14536-5522 (=Swift J1453.4-5524). The photometry, polarimetry and spectroscopy are modulated on an orbital period of 3.1564(1) hours. Orbital circularly polarized modulations are seen from  $\sim 0$  to  $\sim -18$  per cent, unambiguously identifying IGRJ14536-5522 as a polar. The negative circular polarization is seen over  $\sim 95$  per cent of the orbit, which is consistent (as viewed from Earth) with a single pole accretor. We estimate some of the system parameters by modeling the polarimetric observations.

Some of the high speed photometric data show modulations that are consistent with quasi-periodic oscillations (QPOs) on the order of 5-6 minutes. Furthermore, for the first time, we detect the (5-6) minute QPOs in the circular polarimetry. We discuss the possible origins of these QPOs. In addition, we note that the source undergoes frequent changes between different accretion states.

We also include details of HIPPO, a new high-speed photo-polarimeter used for some of our observations. This instrument is capable of high-speed, multi-filtered, simultaneous all-Stokes observations. It is therefore ideal for investigating rapidly varying astronomical sources such as magnetic Cataclysmic Variables.

**Key words:** accretion, accretion discs – methods: analytical – techniques: polarimetric – binaries: close – novae, cataclysmic variables – X-rays: stars.

## 1 INTRODUCTION

The standard picture of a cataclysmic variable (CV) is a binary system consisting of a Roche lobe filling red dwarf (known as the secondary or the donor star) and an accreting white dwarf (the primary). CVs have orbital periods of typically a few hours, and mass transfer is caused by angular momentum loss - see e.g. Warner (1995) for a review of cataclysmic variables. Approximately 20% of the known CVs are magnetic cataclysmic variables (mCVs), where the white dwarf has a strong magnetic field (see the catalogue

of Ritter & Kolb 2003). These are further sub-divided into two subtypes, namely intermediate polars (IPs) and polars, depending on the strength of the magnetic field of the white dwarf and the degree of synchronism between the white dwarf spin and the binary orbit- see the reviews given by Cropper (1990) and Patterson (1994).

In polars, also known as AM Her systems, the white dwarf has a sufficiently strong magnetic field to lock the system into synchronous rotation and to prevent completely the formation of an accretion disc. Instead, the material from the secondary overflowing the Roche lobe initially falls towards

the white dwarf following a ballistic trajectory until, at some distance from the white dwarf, the magnetic pressure overwhelms the ram pressure of the ballistic stream, confining the flow until it eventually reaches the surface where it forms a hot shocked region.

It has long been known that CVs are a significant source of soft (< 2 keV) and medium energy (2-10 keV) X-rays (e.g. Patterson et al. 1984). Recent surveys with INTEGRAL show that CVs are also notable sources of hard (> 20 keV) X-rays. A large fraction of these are made up of magnetic CVs and in particular IPs (see Barlow et al. 2006 and Revnivtsev et al 2008). Interestingly, out of the five asynchronous polars known, two are INTEGRAL sources.

IGRJ14536-5522 (=Swift J453.4-5524) was discovered as a hard X-ray source by INTEGRAL (Kuiper, Keek, Hermsen, Jonker & Steeghs 2006) and by Swift/BAT (Mukai et al. 2006). A pointed Swift/XRT observation led to the identification with a ROSAT all-sky survey (RASS) source 1 RXS J145341.1-552146, and hence to its optical identification (Masetti et al. 2006). Revnivtsev et al. (2008) classify it as an IP.

Follow-up spectroscopy and photometry with SALT (Southern African Large Telescope) and with the SAAO (South African Astronomical Observatory) 1.9m telescope showed that this object belongs to a rare subtype of magnetic CV: a hard X-ray bright polar or a soft intermediate polar (Mukai, Markwardt, Tueller, Buckley, Potter, Still et al. 2006). Further observations were clearly needed.

Here we report on our optical photo-polarimetric and spectroscopic observations of IGRJ14536-5522. The paper is structured as follows: In Sect. 2 we describe the overall design of a new high speed photo-polarimeter used for some of our observations. Sect. 3 gives an account of all our observations, followed by our analysis of the spectroscopic and photo-polarimetric observations in Sects. 4 and 5 respectively. We finish with a discussion and summary in Sect. 6.

## 2 THE HIGH SPEED PHOTO-POLARIMETER (HIPPO)

SAAO's HIPPO was designed and built in order to replace its highly successful but aging single channel equivalent, namely the UCT (University of Cape Town) photo-polarimeter (Cropper 1985). Its purpose is to obtain simultaneous all-Stokes parameters, multi-filtered observations of unresolved astronomical sources. In addition, it is capable of high speed photo-polarimetry in order to permit investigations of rapidly varying polarized astronomical sources. Of particular interest are magnetic Cataclysmic Variables (mCVs). This is the first refereed publication of the instrument and therefore we describe the overall instrument design, data acquisition and reduction here.

### 2.1 The optical design

Fig. 1 shows a schematic diagram of the optical layout of the polarimeter. Light from the telescope first encounters a field lens that produces a collimated beam. Within the collimated beam is placed a polarizing calibration filter wheel followed

by super-achromatic 1/4 and 1/2 wave-plates. The polarizing calibration filter wheel consists of 2 linear polaroids, 1 circular polaroid (a linear followed by a 1/4 wave plastic retarder to produce a circularly polarized beam), a Lyot depolarizer and an open position. These filters are used for calibration and efficiency measurements of the instrument and/or the telescope. The 1/4 and 1/2 wave-plates are also placed in the collimated beam in order to minimise any lateral modulation of the pupil image as the wave-plates are rotated. A Thompson beam-splitter then produces the ordinary and extraordinary beams. All of the above polarizing optics are placed before any filters or apertures, to avoid problems caused by metallic apertures or filters with residual stress birefringence.

Each beam has its own neutral density, colour filter and aperture wheels. The beams are focused at the aperture wheels by lenses at the top of each channel. Fabry lenses re-image the pupil onto two photo-multiplier tubes. There is also an eye-piece (used for initial alignment) and a dark slide on each channel.

The wave-plates are contra-rotated at 10Hz and therefore modulate the ordinary and extraordinary beams. The modulation is sufficiently rapid that errors which arise as a result of variable atmospheric conditions or telescope guiding modulations are much reduced. In addition, modulations that occur as a result of wedge shaped rotating elements, dirt on the rotating components or dichroism from refraction at the element surfaces appear mostly at harmonics that do not affect the measurement of polarization. The remaining sources of error are photon statistics, which can be minimised by collecting a larger number of photons, and instrument/telescope polarization, which can be measured by observing polarized and un-polarized standard stars in combination with the calibration filters. This recipe for measuring polarimetry is based on the work of Serkowski (1974). Measurements of all the Stokes parameters are made simultaneously from the modulated beams. As both beams are modulated, each provides an independent measurement of the polarization. Therefore, simultaneous two filter observations are possible. Linear- and circular-only modes are also possible by rotating only the 1/2 or 1/4-wave-plates respectively.

Serkowski (1974) provides the formalism for calculating the Stokes parameters from O and E beams that are modulated as a result of passing through two retarders in series. In our case, for constantly contra-rotating 1/4 and 1/2 wave-plates in series, the modulated intensities are given by

$$I'_O = \frac{1}{2} \left( I + \frac{1}{2} Q [\cos 8\Psi_8 + \cos 4\Psi_4] + \frac{1}{2} U [\sin 8\Psi_8 - \sin 4\Psi_4] - V [\sin 6\Psi_6] \right)$$

$$I'_E = \frac{1}{2} \left( I + \frac{1}{2} Q [-\cos 8\Psi_8 - \cos 4\Psi_4] + \frac{1}{2} U [-\sin 8\Psi_8 + \sin 4\Psi_4] + V [\sin 6\Psi_6] \right)$$

for the O and E beams respectively. Where

$$\begin{aligned} \Psi_8 &= 8\Psi - 4C^{(\frac{1}{2})} + 4C^{(\frac{1}{4})} \\ \Psi_6 &= 6\Psi - 4C^{(\frac{1}{2})} + 2C^{(\frac{1}{4})} \end{aligned}$$

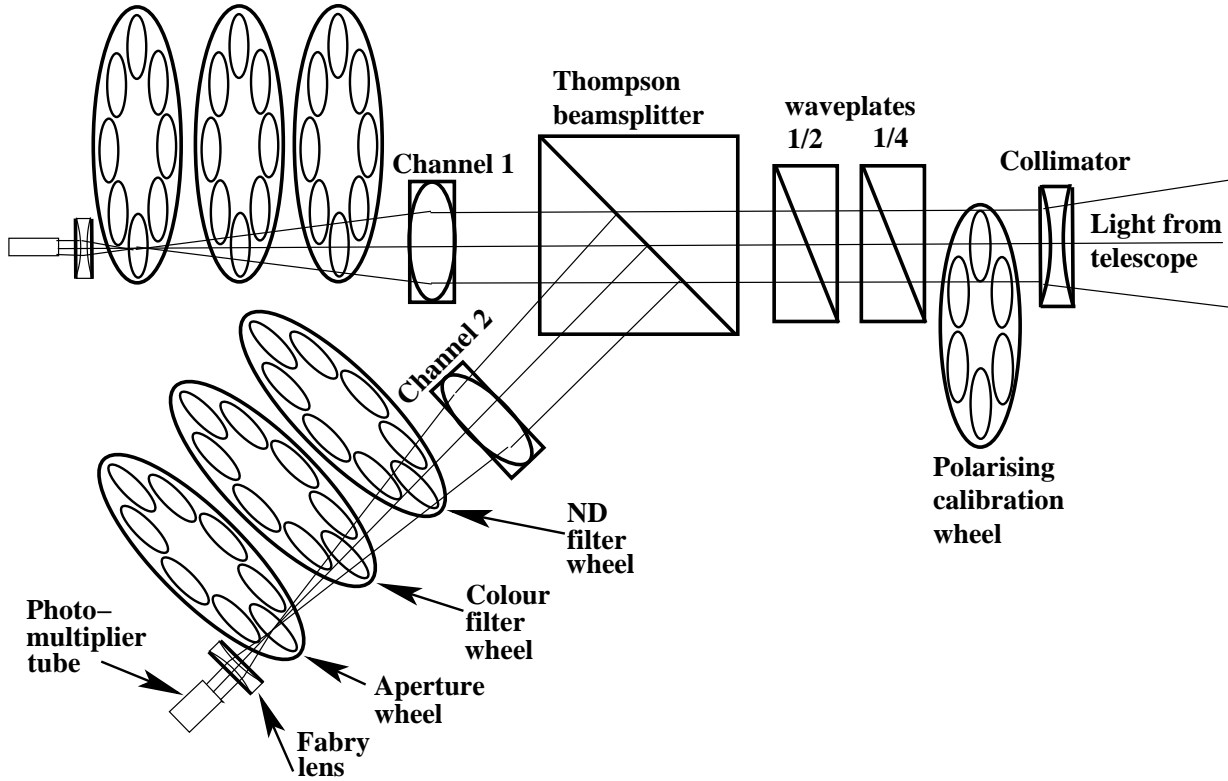


Figure 1. Optical layout of the polarimeter. Channel 1 is a copy of channel 2.

$$\Psi_4 = 4\Psi - 4C^{(\frac{1}{2})}$$

and  $\Psi$  is the angle between the fast axis of the two waveplates and referenced to the 1/4 wave-plate fast axis.  $C^{(\frac{1}{2})}$  and  $C^{(\frac{1}{4})}$  are the zero point constant offsets for the 1/2 and 1/4 wave-plates respectively, and I, Q, U and V are the Stokes parameters. From these equations one can see that the linear component of the polarization is modulated equally at the 4th and 8th harmonics of the rotation frequency. The circular component is modulated at the 6th harmonic. The linear polarization is measured by adding the amplitudes of the 4th and 8th harmonics and, similarly by measuring the 6th harmonic for the circular polarization. A least squares algorithm is used to obtain the amplitudes and phases of the harmonics. Correction factors are applied to each harmonic in order to compensate for the fact that the modulated signal is made up of a finite number of bins (100). Efficiency factors, to compensate for the slight wavelength dependence in retardance of the wave-plates and instrumental polarization, are measured by observing polarized and unpolarized standard stars.

## 2.2 Data acquisition and reductions

The control and data acquisition software is written in C and is hosted by an industrial PC. The photometer counts (X2), minute and second time pulses and 1/2+1/4 wave-plate pulses are handled by real time C code in order to ensure correct and absolute timely recording of the data. The real time code is driven by a 1 milli-second time interval interrupt driven by a 1KHz signal from the time service provided by the Observatory. At every interrupt, the sta-

tus of the waveplate pulses, time pulses and the photometer buffers are recorded. These data are then sent to the user C code, where on-the-fly data reductions are performed. The 1 milli-second data stream is also saved to disk for later off-line data reduction. With a data rate of 1KHz, the 10Hz rotating wave plates are sampled 100 times per revolution. Therefore every 0.1 seconds a polarization measurement is made. Off-line data reductions permit binning of the data to any integer multiple of 0.1 seconds.

## 3 OBSERVATIONS

Table 1 shows a log of all the observations of IGRJ14536-5522.

### 3.1 Optical Spectroscopy

Spectroscopic observations of IGRJ14536-5522 were made during July 2007, on the 1.9-m telescope located on the Sutherland site of the South African Astronomical Observatory (SAAO), using the Cassegrain spectrograph with the SITe1 CCD ( $1752 \times 266 \times 15 \mu\text{m}$  pixels). The higher resolution grating was chosen in order to cover the  $H\beta$ , HeII and  $H\gamma$  emission lines. The lower resolution grating was chosen in order to cover a broader optical wavelength range. Flat field spectra were obtained at the beginning and/or end of each night and wavelength calibration was provided by observing a CuAr lamp approximately every 20-25 minutes. Spectrophotometric flux standards were also observed, allowing flux calibration. Data reductions made use of the standard tools available through IRAF.

**Table 1.** Table of observations. Cass Spect is the Cassegrain spectrograph, 1.9m and HIPPO are the 1.9m telescope and the High speed Photo-Polarimeter respectively of the South African Astronomical Observatory. OG570 and BG390 are broad-band red and blue filters respectively. SALTICAM is the CCD camera of the Southern African Large Telescope. UCTCCD is the University of Cape Town CCD camera. RSS is the Robert Stobie Spectrograph. Observed bright and faint states are indicated by <sup>h</sup> and <sup>l</sup> in the last column. <sup>M</sup> denotes observations originally published in Mukai et al. 2006.

Date	Telescope	Instrument	Spectral range/ filter	Resolution (Å)	No. of spectra	Integration times(s)	Dataset length (orbits)
14/15 Sep 2006	1.9m	UCT CCD	Clear	-	-	60	~ 0.85 <sup>hM</sup>
15/16 Sep 2006	1.9m	UCT CCD	Clear	-	-	60	~ 0.37 <sup>hM</sup>
17/18 Sep 2006	1.9m	UCT CCD	Clear	-	-	60	~ 0.72 <sup>hM</sup>
18/19 Sep 2006	1.9m	UCT CCD	Clear	-	-	60	~ 0.82 <sup>hM</sup>
14-9 May/Jun 2006	SALT	RSS	5930-7212Å	1	31	600	~ 0.9 <sup>lM</sup>
6/7 Jul 2007	1.9m	Cass Spect	4000-5000Å	1	42	600	~ 2.1 <sup>h</sup>
8/9 Jul 2007	1.9m	Cass Spect	4000-5000Å	1	42	600	~ 2.1 <sup>h</sup>
9/10 Jul 2007	1.9m	Cass Spect	4000-5000Å	1	39	600	~ 2.0 <sup>h</sup>
10/11 Jul 2007	1.9m	Cass Spect	3750-7800Å	4	42	500	~ 2.0 <sup>h</sup>
25/26 Jul 2007	1.9m	Cass Spect	4000-8000Å	4	9	1200	~ 1.0 <sup>l</sup>
27/28 Feb 2008	1.9m	HIPPO	Unfiltered	-	-	1ms,0.1	~ 1.2 <sup>h</sup>
28/29 Feb 2008	1.9m	HIPPO	OG570, BG39	-	-	1ms,0.1	~ 1.2 <sup>h</sup>
29/1 Feb 2008	SALT	SALTICAM	Clear	-	-	0.1	~ 0.35 <sup>h</sup>
1/2 Mar 2008	SALT	SALTICAM	Clear	-	-	0.1	~ 0.15 <sup>h</sup>
1/2 Mar 2008P	1.9m	HIPPO	B,I	-	-	1ms	~ 1.2 <sup>h</sup>
2/3 Mar 2008	SALT	SALTICAM	Clear	-	-	0.1	~ 0.17 <sup>h</sup>
2/3 Mar 2008	1.9m	HIPPO	B,R	-	-	1ms	~ 1.2 <sup>h</sup>
3/4 Apr 2008	1.9m	HIPPO	B,I	-	-	1ms, 0.1s	~ 1.2 <sup>h</sup>
5/6 Apr 2008	1.9m	HIPPO	B,V,R,I	-	-	1ms, 0.1s	~ 1.5 <sup>h</sup>
7/8 Apr 2008	1.9m	HIPPO	Clear,B,I	-	-	1ms, 0.1s	~ 1.2 <sup>h</sup>
7/8 May 2008	SALT	SALTICAM	U	-	-	0.1	~ 0.13 <sup>h</sup>
7/8 May 2008	SALT	SALTICAM	B	-	-	0.1	~ 0.26 <sup>h</sup>
9/10 May 2008	SALT	SALTICAM	V	-	-	0.1	~ 0.23 <sup>h</sup>
13/14 May 2008	SALT	SALTICAM	R	-	-	0.1	~ 0.3 <sup>h</sup>
17/18 May 2008	SALT	SALTICAM	B	-	-	0.1	~ 0.26 <sup>h</sup>
18/19 May 2008	SALT	SALTICAM	V	-	-	0.1	~ 0.1 <sup>h</sup>

SALT RSS spectra were obtained when the system was in a lower state between May 14 and Jun 9 2006. These observations were presented in Mukai et al. (2006) and have been listed here for completeness and for comparison.

### 3.2 Optical Polarimetry

IGRJ14536-5522 was observed polarimetrically on the SAAO 1.9m telescope during the commissioning week of the HIPPO in February and March 2008 and then later in April 2008. The HIPPO was operated in its simultaneous linear and circular polarimetry and photometry mode (All-Stokes). White light observations (3500-9000Å) were defined by the response of the two RCA31034A GaAs photomultiplier tubes, whilst for others a broad blue band (3500-5500Å) BG39 filter, a broad red band (5700-9000Å) OG570 filter, or B,V,R,I filters were used.

Several polarized (HD80558, HD111579, HD111613, HD147084, HD126593, HD147084, HD160529, HD298383, HD110984) and non-polarized (HD90156, HD100623) standard stars (Hsu & Breger 1982 and Bastien et al. 1988) were observed in order to calculate the position angle offsets, instrumental polarization and efficiency factors. Background sky polarization measurements were also taken at frequent intervals during the observations. Data reduction then proceeded as outlined in the previous sections.

### 3.3 Optical Photometry

IGRJ14536-5522 was observed photometrically with the UCTCCD in 2006, as part of the polarimetric observations in 2008 and with SALTICAM in 2008. The observations are not absolutely photometrically calibrated.

## 4 SPECTROSCOPIC ANALYSIS

### 4.1 The mean spectrum

Fig. 2 shows the average of the spectra taken when the system was in a higher state (upper spectrum) and when it was observed to be in a lower state two weeks later during July of 2007 (lower spectrum). These observations were made with the SAAO 1.9m telescope. The higher state spectrum is very typical for a polar (see e.g. QS Tel: Rosen et al. 1996, HU Aqr: Schwope, Mantel & Horne, 1997), i.e. it exhibits Balmer emission lines (H $\alpha$  - H11) as well as neutral helium (He I  $\lambda\lambda$  4026, 4387, 4471, 4713, 4922, 5016, 5048, 5876, 6678, 7065Å), ionised helium (He II  $\lambda\lambda$  4542, 4686, 5411). CaII (3933Å), blended CIII, OII, NIII (4640Å) and FeI (5172Å). The phase-resolved low-resolution spectra clearly display bright and faint phases (not shown).

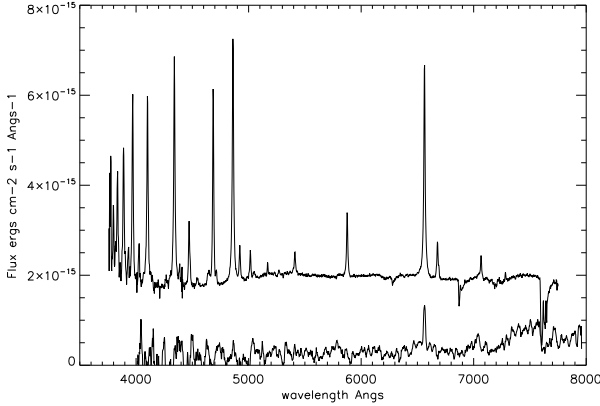


**Figure 2.** Average of the low resolution spectra. Upper and lower average spectra are made from the observations taken on 10/11 (during a higher state) and the 25/26 (during a lower state) July 2007, respectively. The lower state data has been magnified by 10.

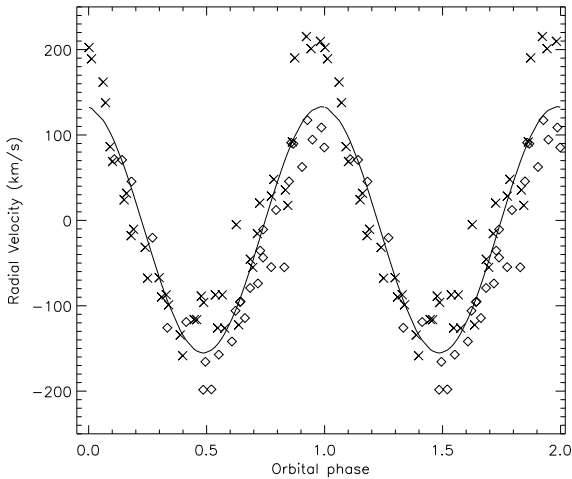


**Figure 3.** The  $H\alpha$  radial velocity curve of IGRJ14536-5522 folded on the 3.1564 hr period with arbitrary phasing. Crosses and diamonds are the higher state 2007 and the lower state 2006 observations respectively.

#### 4.2 A spectroscopic ephemeris for the secondary.

We measured the radial velocity of the  $H\alpha$  emission line in our July 2007 observations using a single Gaussian convolution method. These results were then combined with the same measurements made by Mukai et al (2006) of their June 2006 observations. A  $\chi^2$  minimization technique was then used in order to search for any periods. A period of 3.1564(1) hours was detected which is consistent with that found by Mukai et al (2006) and recognized as the orbital period. The period error arises as a result of not being able to distinguish between aliases.

Fig. 3 shows the  $H\alpha$  radial velocity curve folded on the 3.1564 hr period with arbitrary phasing. We measure a gamma velocity of  $-7.3(1)$  km/s and a semi-amplitude of  $144.9(2)$  km/s. The numbers in brackets are the one sigma standard deviations of a sine fit to the radial veloc-

ities. The higher and lower state data are distinguished by the crosses and diamonds respectively. Note that the higher state data appears to have a generally higher velocity than the lower state data. We attribute this to different emission regions contributing to the line emission when in different states: the irradiated face of the secondary star dominates the emission line profile during lower states, but the emission lines become multi-component during higher states (see e.g. UW Pic: Romero-Colmenero et al. 2003). Hence the multi-component nature of the emission lines have probably biased our gamma velocity measurement due to asymmetric line profiles.

In order to derive a zero point for the ephemeris we analysed our higher resolution spectroscopic data. Fig. 4 shows these data, taken in July 2007, phased and folded on the above detected period and centered on the HeII 4686Å line. These observations show the multi-component nature more clearly (described in more detail below). In particular, a bright narrow component can be seen (indicated by the dashed curve), which is commonly associated with the irradiated face of the secondary star. We fitted multi(3)-Gaussian profiles to the trailed spectra and calculated the radial velocities of the 3 visible components as a function of phase. A best sinusoidal fit to the narrow component was used in order to derive the time of blue-red crossing and hence the time of inferior conjunction of the secondary star. Accordingly, this in turn is used to give the epoch to our ephemeris:

$$T(HJD) = 2454290.14723(8) + 0.131517(4)E$$

The number enclosed in brackets (on the epoch) is the formal one sigma error measurement. However we note that the true superior conjunction of the secondary may be offset by a value that is larger than the quoted error if the irradiated face of the secondary is not symmetric about the line of centers of the two stars.

We measure a gamma velocity and semi-amplitude of  $-26.0(3)$  km/s and  $80.8(4)$  km/s respectively for the narrow component. The numbers in brackets are the one sigma standard deviations of a sine fit to the radial velocities. Henceforth, all our observations are phased on the above ephemeris.

#### 4.3 The trailed spectra and Doppler tomograms

Fig. 4 shows our HeII trailed spectra, the corresponding Doppler tomogram (Marsh & Horne 1988) and the reconstructed trailed spectra of IGRJ14536-5522. The spectra were phase-folded on the ephemeris derived above, continuum subtracted and then the Doppler tomography code of Spruit (1998) was used.

We have also calculated  $H\beta$  and  $H\gamma$  Doppler tomograms (not shown). These were found to be very similar to the HeII Doppler tomogram, but the trailed spectra do not show the narrower components as clearly. Therefore we present only the HeII observations and the corresponding interpretation.

The HeII trailed spectra clearly display the multiple components that have been seen to some extent in other polars (e.g. Schwöpe et al. 1995 and Rosen et al. 1996). From Fig. 4, a narrow component (indicated by the dashed curve)

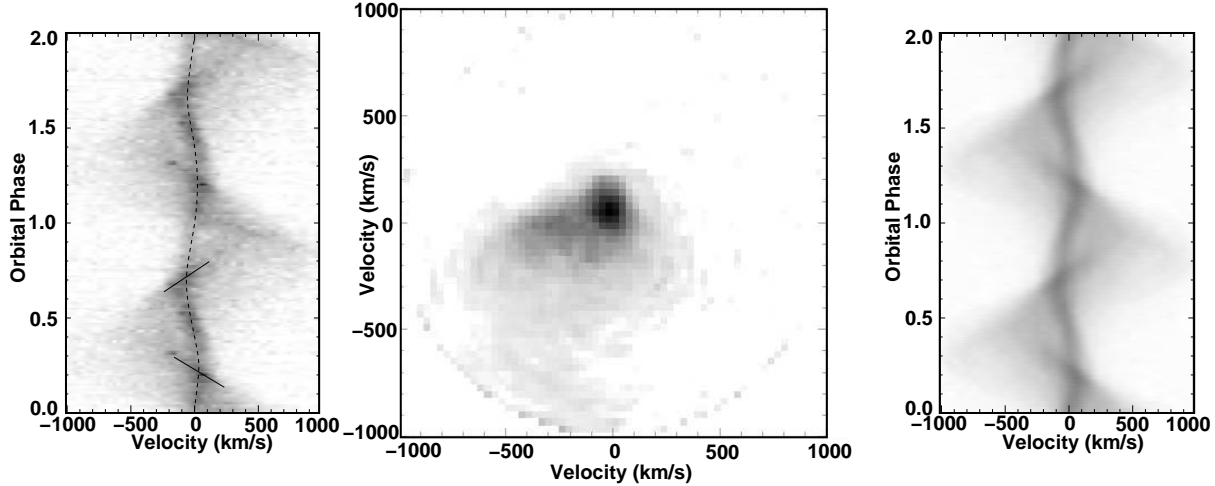


**Figure 4.** From left to right: HeII trailed spectra phase-folded on the derived ephemeris, the resulting Doppler tomogram and the reconstructed trailed spectra.

is visible throughout the whole orbit and is generally recognised as emission from the irradiated face of the secondary star. The fact that it is visible throughout the whole orbit suggests a relatively low inclination, although the radial velocity amplitudes are consistent with more moderate inclinations (see e.g. V834 Cen: Potter et al. 2004).

There is possibly a second narrow component that is most visible where it crosses and merges (indicated by diagonal lines) with the narrow component from the secondary at phases  $\sim 0.25$  and  $\sim 0.75$ . There also appears to be a broad but fainter underlining component that reaches maximum blue-shift velocities of  $\sim -1000$  km/s at phase  $\sim 0.5$  and it remains discernible with maximum redshift just before phase  $\sim 1.0$ . This fits the general picture of emission from a ballistic accretion stream which then accelerates and becomes magnetically channeled before reaching the surface of the white dwarf (producing the broad component).

The HeII Doppler tomogram in Fig. 4 shows the typical features of a moderately inclined polar. In particular, emission is seen at the expected location of the irradiated face of the secondary, approximately centered on x-velocity  $\sim 0$  km/s and y-velocity  $\sim 100$  km/s. The x-velocity appears to be slightly negative offset from 0. This can be explained as being due to the leading edge of the secondary being more illuminated by the hot accretion region on the surface of the white dwarf, which also leads in orbital phase (e.g. V834 Cen: Potter et al 2004), although we cannot rule out that it may also be as a result of inaccuracies in the determination of the gamma velocity and/or the phasing of inferior conjunction on the secondary. The tomogram also shows emission at the expected location of the ballistic accretion stream, seen to start at roughly the location of the secondary and curving away towards more negative x and y-velocities. There is also a very faint underlying component seen protruding from zero velocities to low negative velocities. This has also been seen in other polars (e.g. Hu Aqr: Schwope, Mantel & Horne 1997) and is generally explained as emission from accreting material where it starts to be threaded by the magnetic field of the white dwarf.

## 5 PHOTO-POLARIMETRIC ANALYSIS

### 5.1 The Photometry

The left hand plots of Fig. 5 show the photometric observations of IGRJ14536-5522 taken on the 5th (top 4 plots) and 7th of April 2008 (last plot), phased on the spectroscopic ephemeris derived in section 4.2. The 5th of April observations were obtained by interleaving 60 second integrations between the B and V filters and the R and I filters on channels 1 and 2 of the polarimeter respectively. They are, therefore, effectively simultaneous. Conditions were photometric during these observations. The source was in a higher state.

#### 5.1.1 The orbital modulation and the dip

As can be seen from Fig. 5, the orbital modulation is single-humped, which can be attributed to the beaming of cyclotron emission from a single accretion spot on the surface of the white dwarf. The orbital intensity minimum occurs when the emission region is most face-on. The single humped morphology also implies a moderate inclination for the system (see e.g. Ferrario & Wickramasinghe (1990) and Potter, Hakala & Cropper (1998)).

The orbital intensity minimum is cut into by a narrow dip at approximately phase  $\sim 0.97$ . This dip is also seen in the polarimetry lightcurves (Fig. 5, right). Considering the accuracy of the phasing of the spectroscopic ephemeris (section 4.2), the narrow dip could be due to an eclipse of the white dwarf by the secondary star. However, this scenario is not consistent with the results of our spectroscopic analysis and polarimetric modeling (section 4.3 and 5.2 respectively), which favour moderate inclinations. Therefore, it is more likely that the dip arises as a result of absorption by material in the accretion stream and/or the accretion column directly above the emission region when we see it most face on (see e.g. Bridge et al. 2002).

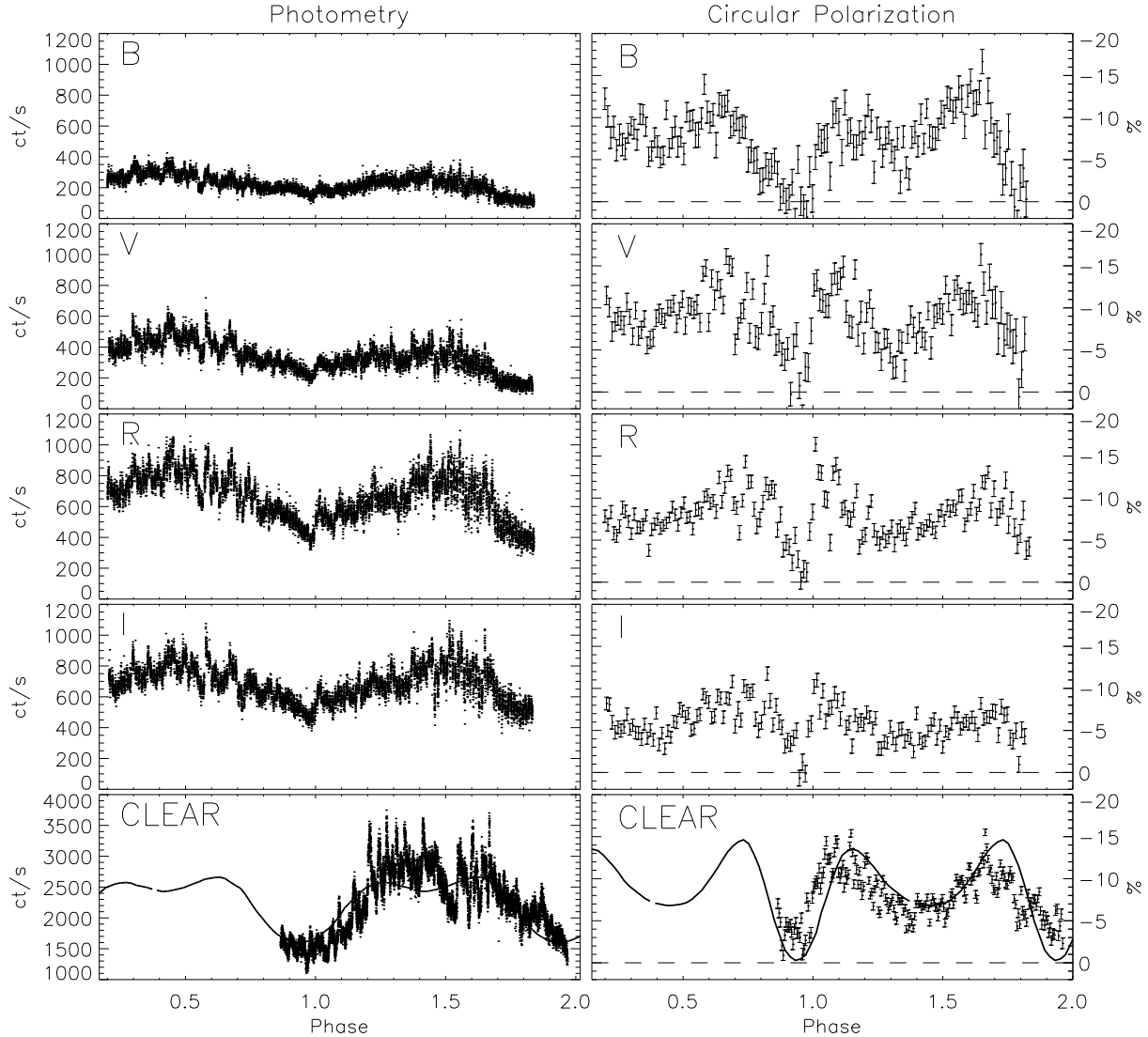


**Figure 5.** The photometric and polarimetric data phased on the spectroscopic ephemeris derived in section 4.2. The upper 4 plots are simultaneous B,V,R and I filtered observations of the 5th of April 2008 whilst the bottom plots were made with the clear filter on the 7th April 2008. Solid curves represent the model fit (see section 5.2).

### 5.1.2 The photometric QPOs and flickering

A close inspection of the photometry in Fig. 5 reveals short period modulations throughout the orbit that are mostly consistent with being due to noise or flickering. However, detailed Fourier analysis of all of our photometry reveals that some of our data sets show significant singularly persistent peaks that are consistent with QPOs.

An example data set is shown in the left (a) plot of Fig. 6 from the 28th February 2008. We analysed the data set by first splitting it into  $\sim 40$  minute sections with an overlap of 85 percent. Next, each section of data was normalised to a best fit second order polynomial before being subjected to Fourier analysis. The results are shown as a trailed amplitude spectrum in the left (b) plot of Fig. 6. In this grey scale plot the darker areas correspond to larger amplitudes. Between phases 0.2-1.0 the amplitude spectra do not show any significant peaks which indicates that the variations are mostly flickering or noise. However, there is a significant

dominating signal centered on 0.0032(1) Hz (5.2 minutes, indicated by the dashed line) between the phases 1.0 and 1.3. This is clear evidence of a QPO. The 7 April 2008 data set also shows clear evidence of a QPO (Fig. 7, left (a+b) plots) at a similar period (0.0028(1) Hz,  $\sim 5.9(3)$  minutes) centered on the same phase range ( $\sim 1.2$ ) as well as a lower harmonic (0.00136(15) Hz), both indicated with dashed lines.

In the left (c) plot of Fig. 6 we show the normalised photometry during the phase range that is dominated by the QPO. Overplotted are the least squares fit of the QPO frequencies. As one can see, the 28 February photometric QPO is very well described by the single dominant frequency as found in the trailed amplitude spectra. The 7 April 2008 photometric QPO (Fig. 7, left (c) plot) shows a more variable amplitude compared to the 28 February QPO. This then explains why the trailed amplitude spectra shows two frequencies for the QPO, one being the harmonic of the other. The left (d) plots of Figs. 6 and 7 show the corre-

sponding amplitude spectra for the QPO dominated phase range. The QPOs are discussed further in section 6.2.

## 5.2 The Polarimetry

The right hand plots of Fig. 5 show the polarimetric (circular) observations of IGRJ14536-5522 taken on the 5th (top 4 plots) and 7th of April 2008 (bottom plot), phased on the spectroscopic ephemeris derived in section 4.2. These were generated from the same dataset as the photometry presented in the left hand plots. We were unable to detect any linear polarization.

The circular polarization curve is double-humped and negative throughout the entire orbit, which is consistent with emission from a single accretion region in a moderately inclined system. The polarization reaches maximum negative values of  $\sim 15$  percent, with the peaks of the humps occurring at orbital phases  $\sim 0.1$  and  $\sim 0.7$ . There is also a narrow dip at phase  $\sim 0.97$ , where the polarization reaches a minimum of zero. This is coincident with the narrow dip seen in the photometry, thus supporting the hypothesis that the emission being absorbed is cyclotron radiation from the accretion region (section 5.1.1). The phasing of the dip implies that the location of the accretion region must be close to the line of centers of the two stars. In addition, there is a broad minimum centered on the narrow dip, which is typically caused by the beaming of the cyclotron radiation at those phases where the line of sight most closely approaches the axis of the column (Barret & Chanmugam 1984; Wickramasinghe & Meggitt 1985).

### 5.2.1 The system geometry

We investigated the system geometry further by modeling the photo-polarimetry. We constructed a single arc model assuming accretion along dipole field lines as in Potter et al (1997). A magnetic field of 20MG was assumed and the cyclotron flux was calculated using the stratified accretion shock grids of Potter, Ramsay, Wu & Cropper (2002). We considered only the clear filter data because there does not appear to be any obvious wavelength dependence in the multi-filtered observations. Consequently, different values for the magnetic field strength and different shock models cannot be investigated. However, the results of this model are largely independent of our choice of the magnetic field strength.

The values for the parameters describing the inclination, dipole offset angle and location, shape and size of the accretion region were explored by comparing each resulting lightcurve to the data. The most successful set of parameters integrated the emission from an arc shaped region extending from  $170^\circ$  to  $230^\circ$  in magnetic longitude and  $10^\circ$  from the magnetic pole with a system inclination of  $50^\circ$ . The magnetic dipole was offset by an angle of  $10^\circ$  from the white dwarf spin axis. A constant unpolarized background of 1000ct/s was assumed.

We found that the model gave poor reproductions of the data for inclinations outside a range of  $45\text{--}55^\circ$ , when either the extent in phase or the double humped morphology of the circular polarization were poorly reproduced. The solid curves in the lower 2 plots of Fig. 5 show the results of the

best model parameters over-plotted on the observations. The model has the accretion region most face on at phase  $\sim 0.95$  and least face on at phase  $\sim 0.45$ .

### 5.2.2 The polarized QPOs and flickering

We analysed our circular polarimetric data in the same manner as that of the photometry. The data and results for the 28 February 2008 are shown in the right hand plots of Fig. 6. As can be seen from the right (b) plot, the trailed amplitude spectra is consistent with mostly noise and/or flickering between phases 0.2-1.0. However a QPO centered on 0.0031(1) Hz (5.4(3) minutes) is clearly evident between phases 1.05-1.2. The QPO period is consistent within the errors to that of the photometric QPO.

The right hand plots of Fig. 7 show the Fourier analysis of the circular polarimetric data taken on 7 April 2008. Once again, the trailed amplitude spectra displays the same characteristics as the photometry, i.e. a dominant frequency is seen to be centered on 0.0028(1) Hz (5.9(3) minutes) and a lower harmonic at 0.0015(1) Hz (both indicated by dashed lines) during the phase range 1.0-1.3.

In the right (c) plots of Fig. 6 and Fig. 7 we show the normalised circular polarimetry during the phase range that is dominated by the QPOs. Overplotted are the least squares fit of the QPO frequencies. As one can see, the circularly polarized QPOs share the same characteristics as the photometric QPOs, namely the 28 February circularly polarized QPO is very well described by the single dominant frequency found in the trailed amplitude spectra. Furthermore the 7 April 2008 circularly polarized QPO shows a more variable amplitude compared to the 28 February QPO, thus requiring a harmonic frequency to better characterise the data. The QPOs are discussed further in section 6.2.

## 6 DISCUSSION AND SUMMARY

### 6.1 Object classification and system geometry

Our optical spectroscopy and high speed photo-polarimetry of the INTEGRAL source IGRJ14536-5522 (=Swift J453.4-5524) unambiguously confirm its identification as a polar. Negative circular polarization is seen over all of the orbit, which is consistent with a single pole accretor at a moderate inclination. We estimate some of the system parameters by modeling the polarimetric observations. The most successful model integrated the emission from an arc-shaped region extending from  $170^\circ$  to  $230^\circ$  in magnetic longitude and  $10^\circ$  from the magnetic pole. The system inclination was found to be in the range of  $45\text{--}55^\circ$  with a magnetic dipole offset angle of  $10^\circ$ .

### 6.2 The QPOs and flickering

Our high speed photo-polarimetry shows flickering on minute time-scales. Furthermore, for the first time, we detect QPOs in the photometry and circular polarimetry.

Photometric variations on the time scales of minutes are a common feature of many polars, from X-rays to infrared (e.g. Szkody & Margon 1980 and Watson, King & Williams



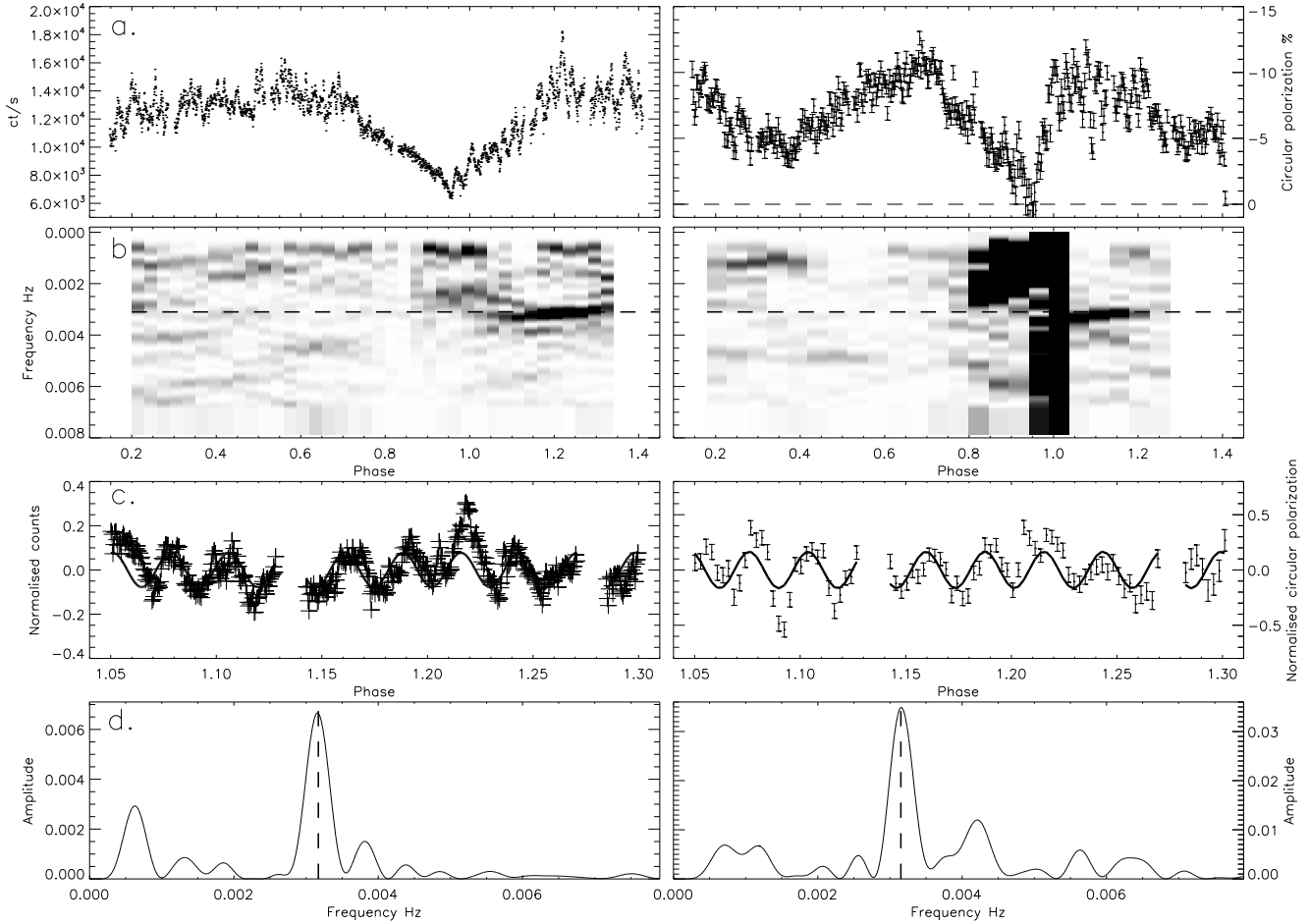


**Figure 6.** Left plots, a-d: The photometry, the corresponding trailed amplitude spectra, the normalised photometry for the phase range 1.0-1.3 and its corresponding amplitude spectra respectively. The solid curve is the least squares fit using the frequency derived from the trailed spectra (dashed line). Right plots: as in the left plots but for the circular polarization. Data set from 28 February 2008.

1987), and have been characterised as flickering, fluctuations, QPOs or erratic QPOs according to different authors. In general (although not always strictly true), QPOs describe variations that show some coherence over a period of time. They mainly cluster in time-scales in the range of a few seconds (1-5) or minutes (4-10). The (1-5s) QPOs are of low amplitude and have been observed in the optical in only a few polars (e.g. V834 Cen, AN Uma and VV Pup). The larger amplitude (4-10 min) QPOs seem to be a general feature of most polars. By eye, they can appear to show some sort of coherence, but fail to show any significant singularly persistent peaks under Fourier analysis. Instead, groupings of periods are seen and are often referred to as QPO-like. Flickering and fluctuations best describe variations that do not show any periodic behavior.

There is evidence that the 4-10 minute QPOs may consist of the superposition of regular periodic oscillations: Bonnet-Bidaud, Somova & Somov (1991) report on observations of AM Her during an intermediate brightness state where they find fluctuations to be nearly periodic, with a period increasing from 250s to 280s. They reason that they observed AM Her in a transition from bright-state to faint-state where a given accretion rate is able to excite stable

oscillations. Alternatively, during the higher state, many oscillations may be present but masked by the superposition of different modes corresponding to different accretion tubes. Therefore, during the transition, the accretion rate decreases, reducing the number of accretion tubes until finally only one unique tube contributes to the emission.

Ultimately, the photometric oscillations are caused by variations in the accretion flow. There are several theories/models that attempt to explain the variations. King (1989) remarks that the (4-10 minute) periods are characteristic of a dynamical time at the photosphere of the companion. Irradiation of the region near the  $L_1$  point will result in the formation of an ionisation front, which will tend to oscillate and therefore modulate the accretion. Other models involve the capture of inhomogeneities of the accretion flow at the capture radius (Kuijpers and Pringle 1982) and accretion gate mechanisms (Patterson et al. 1981).

The short period QPOs (1-5s) have been observed in  $\sim 6$  systems (e.g. V834 Cen, AN Uma and VV Pup). Langer, Channugam & Shaviv (1982) realised that the 1-5s oscillations were consistent with the cooling time-scales for white dwarf-radiated shock waves and thus QPOs are potentially powerful probes of the radiative shocks. Observations of

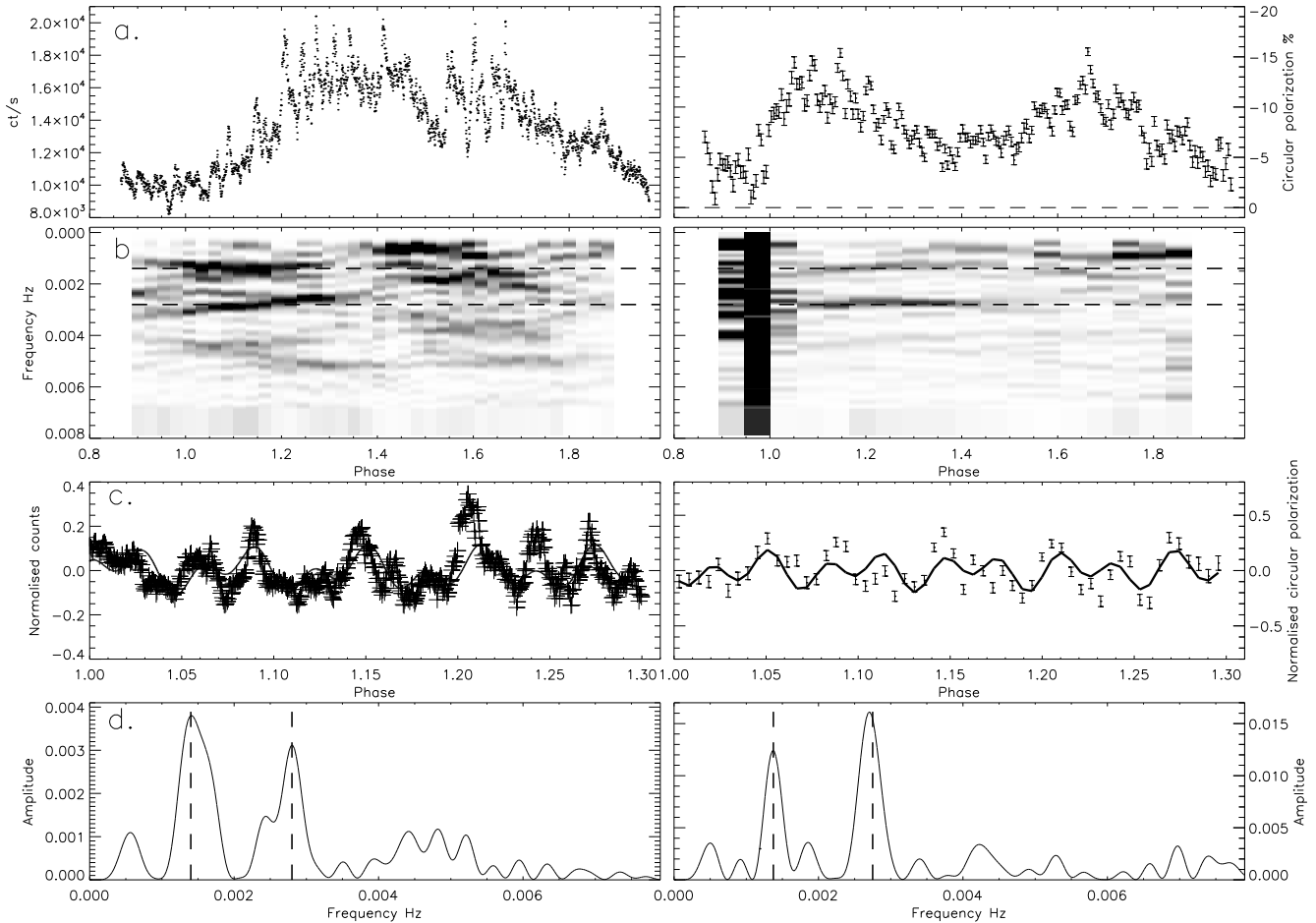


**Figure 7.** As in Fig 6 for the 7 April 2008 data set.

VV Pup (Larson 1989) demonstrated conclusively that the QPOs arose in a region near the shock emission region on the white dwarf.

From our results presented in Figs. 6 and 7 it is clear that IGRJ14536-5522 exhibited photometric and polarized QPOs (5-6 minutes) on two separate occasions. Additionally, the fact that we observe the QPOs oscillations in the polarimetry, unequivocally places the emission site at the cyclotron emitting shock region. Furthermore, the QPOs were seen during phases 1.0-1.3 only. We propose that the super-position of the oscillations arising from numerous accretion tubes (similar to the mechanism of Bonnet-Bidaud, Somova & Somov 1991) applies to IGRJ14536-5522. However, instead of a reduced accretion state leading to a reduced number of accretion tubes, we suggest that for most of the orbit the superposition of emission from many accretion tubes leads to the observed flickering. However during the phase interval 1.0-1.3 we preferentially see the trailing edge of the accretion region as the white dwarf rotates. The leading part of the accretion region is effectively shielded from our view by its trailing edge for this phase interval. Consequently we observe a singular QPO corresponding to a singular accretion tube.

Our observations of IGRJ14536-5522 indicate that it

undergoes relatively frequent changes in accretion state, making it a good candidate for capturing it in transition and testing this scenario further. If QPOs are also present in the X-rays then IGRJ14536-5522 is an ideal source for investigating the two dominating shock cooling mechanisms: i.e. bremsstrahlung and cyclotron cooling.

Finally, we would like to note the importance of optical follow-up observations of candidate CV INTEGRAL sources, in particular with photometry and/or polarimetry. It has been noted that many CVs detected by INTEGRAL are IPs, both new and re-discoveries (see e.g. Barlow et al. 2006 and Revnivtsev et al 2008). However, as Pretorius (2009) points out, it is only through follow-up observations that unequivocal identifications can be made. A case in point is IGRJ14536-5522, which had been assumed to be an IP (see e.g. Revnivtsev et al. 2008) even though a spin period had not been detected.

## 7 ACKNOWLEDGMENTS

We thank the anonymous referee for comments and suggestions that have significantly improved the paper.

This material is based upon work supported financially

by the National Research Foundation. Any opinions, findings and conclusions or recommendations expressed in this material are those of the author(s) and therefore the NRF does not accept any liability in regard to thereto.

Some of the observations reported in this paper were obtained with the Southern African Large Telescope (SALT), a consortium consisting of the National Research Foundation of South Africa, Nicholas Copernicus Astronomical Center of the Polish Academy of Sciences, Hobby Eberly Telescope Founding Institutions, Rutgers University, Georg-August-Universitt Gttingen, University of Wisconsin - Madison, Carnegie Mellon University, University of Canterbury, United Kingdom SALT Consortium, University of North Carolina - Chapel Hill, Dartmouth College, American Museum of Natural History and the Inter-University Centre for Astronomy and Astrophysics, India.

## REFERENCES

- Barlow E. J., Knigge C., Bird A. J., Dean A. J., Clark D. J., Hill A. B., Molina M., Sguera V., 2006, MNRAS, 372, 224
- Barret P. E. & Chanmugam, G., 1984, ApJ, 278, 298
- Bastien P., Drissen L., Menard F., Moffat A. F. J., Robert C. & St-Louis N., 1988, AJ, 95 900
- Bonnet-Bidaud J. M., Somova T. A. & Somov N. N., 1991, A&A, 251, L27
- Bridge C. M., et al., 2002, MNRAS, 336, 1129
- Cropper M. S., 1985, MNRAS, 212, 709
- Cropper M. S., 1990, Space Sci. Rev. 54, 195
- Ferrario L. & Wickramasinghe D. T., 1990, ApJ, 357, 582
- Hsu J. C., Breger M., 1982, ApJ, 262, 732
- King A. R., 1989, MNRAS, 241, 365
- Kuiper L., Keek S., Hermsen W., Jonker P. G. & Steeghs D., 2006, ATel, 684
- Kuijpers J. & Pringle J. E., 1982, A&A, 114, L4
- Langer S. H., Chanmugam C. & Shaviv G., 1982, ApJ, 258, 289
- Larsson S., 1989, A&A, 217, 146
- Marsh T. R. & Horne K., 1988, MNRAS, 235, 269
- Masetti N. et al. 2006, ATel, 783
- Mukai K. et al. 2006, ATel, 686
- Mukai, K., Markwardt, C., Tueller J., Buckley D., Potter S., Still M. & Swift/BAT team, 2006, AAS, 209, 0912
- Patterson P., Williams G. & Hiltner W. A., 1981, ApJ, 245, 618
- Patterson J., Lamb D. Q., Fabbiano G., Raymond J. C., Beuermann K. Swank J. & White N. E. 1984, ApJ, 279, 785
- Patterson J., 1994, PASP, 106, 209
- Potter S. B., Cropper M. S., Mason K. O., Hough J. H., Bailey J. A., 1997, MNRAS, 285, 82
- Potter S. B., Hakala P. J., Cropper M., 1998, MNRAS, 297, 1261
- Potter S. B., Ramsay G., Wu K. & Cropper M., 2002, in Gänsicke B. T., Beuermann K., Reinsch K., eds, ASP Conf. Ser. Vol. 262, The Physics of Cataclysmic Variables and Related Objects, Astron. Soc. Pac., San Francisco, p. 165
- Potter S. B., Romero-Colmenero E., Watson C. A., Buckley D. A. H. & Phillips A., 2004, MNRAS, 348, 316
- Pretorius M. L., 2009, MNRAS, 395, 386
- Romero-Colmenero E., Potter Stephen B., Buckley D. A. H., Barrett P. E. & Vrielmann S., 2003, MNRAS, 339, 685
- Rosen S. R. et al., 1996, MNRAS, 280, 1121
- Szkody P. & Margon B., 1980, ApJ, 236, 862
- Revnivtsev M., Sazonov S., Krivonos R., Ritter H., Sunyaev R., 2008, A&A, 489, 1121
- Ritter H., Kolb U., 2003, A&A, 404, 301 (update RKcat7.9)
- Schwöpe A. D., Thomas H.-C., Beuermann K., Burwitz V., Jordan S. & Haefner R., 1995, A&A, 293, 764
- Schwöpe A. D., Mantel, K.-H. & Horne K., 1997, A&A, 319, 894
- Spruit H. C., 1998, preprint (astro-ph/9806141)
- Serkowski K. 1974, Planets, stars and nebulae studied with photopolarimetry, p. 135 - 174, ed. Gehrels T., University of Arizona, Tucson
- Warner B. 1995, Cataclysmic Variable Stars, Cambridge Astrophysics Series 28, Cambridge University Press
- Watson M. G., King A. R. & Williams G. A., 1987, MNRAS, 226, 867
- Wickramasinghe D. T. & Meggitt S. M. A., 1985, MNRAS, 214, 605